

Measurement of $e^+e^- \rightarrow \pi^+\pi^-$ cross section at CMD-3

I.B.Logashenko^{1,2,a}, R.R.Akhmetshin¹, A.V.Anisenkov¹, V.M.Aulchenko^{1,2}, V.S.Banzarov¹, N.S.Bashtovoy¹, D.E.Berkaev^{1,2}, A.V.Bragin¹, S.I.Eidelman^{1,2}, D.A.Epifanov⁵, L.B.Epshteyn^{1,3}, A.L.Erofeev¹, G.V.Fedotov^{1,2}, S.E.Gayazov^{1,2}, A.A.Grebenuk^{1,2}, D.N.Grigoriev^{1,2,3}, E.M.Gromov¹, F.V.Ignatov¹, S.V.Karpov¹, V.F.Kazanin^{1,2}, B.I.Khazin^{1,2}, A.N.Kirpotin¹, I.A.Koop^{1,2}, O.A.Kovalenko^{1,2}, A.N.Kozyrev¹, E.A.Kozyrev^{1,2}, P.P.Krokovny^{1,2}, A.E.Kuzmenko^{1,3}, A.S.Kuzmin¹, P.A.Lukin^{1,2}, A.P.Lysenko¹, K.Yu.Mikhailov^{1,2}, V.S.Okhapkin¹, Yu.N.Pestov¹, E.A.Perevedentsev^{1,2}, A.S.Popov^{1,2}, G.P.Razuvaev^{1,2}, Yu.A.Rogovsky¹, A.L.Romanov¹, A.A.Ruban¹, N.M.Ryskulov¹, A.E.Ryzhenenkov^{1,2}, V.E.Shebalin¹, D.N.Shemyakin^{1,2}, B.A.Shwartz^{1,2}, D.B.Shwartz^{1,2}, A.L.Sibidanov⁴, P.Yu.Shatunov¹, Yu.M.Shatunov¹, E.P.Solodov^{1,2}, V.M.Titov¹, A.A.Talyshev^{1,2}, A.I.Vorobiov¹, Yu.V.Yudin¹, and Yu.M.Zharinov¹

¹*Budker Institute of Nuclear Physics, SB RAS, Novosibirsk, 630090, Russia*

²*Novosibirsk State University, Novosibirsk, 630090, Russia*

³*Novosibirsk State Technical University, Novosibirsk, 630092, Russia*

⁴*University of Sydney, School of Physics, Falkiner High Energy Physics, NSW 2006, Sydney, Australia*

⁵*University of Tokyo, Department of Physics, 7-3-1 Hongo Bunkyo-ku Tokyo, 113-0033, Japan*

Abstract. Regular operation of the VEPP-2000 electron-positron collider started at the end of 2010 and about 60 pb⁻¹ were collected so far by the CMD-3 detector in the whole available c.m. energy range from 0.32 GeV to 2.0 GeV. One of the main goals of the experiments at VEPP-2000 is a sub-percent measurement of the $e^+e^- \rightarrow \pi^+\pi^-$ cross-section. Here we present the overview of the data analysis techniques and the preliminary results of this measurement.

1 Introduction

One of the least complicated modes of electron-positron annihilation to hadrons, $e^+e^- \rightarrow \pi^+\pi^-$, plays a special role in apparently unrelated physics of the muon's magnetic moment. The non-zero value of the anomalous magnetic moment of muon a_μ is explained by the interaction between muons and virtual fields. Within the framework of the Standard Model there are three contributions to a_μ : QED, electroweak and hadronic. Evaluations of the first two are well under control, but the hadronic contribution cannot be calculated directly due to non-perturbative nature of QCD (for review see [1] and references therein). However, the lowest-order hadronic contribution can be calculated using the dispersion relation:

$$a_\mu^{had;LO} = \left(\frac{\alpha m_\mu}{3\pi}\right)^2 \int_{m_\rho^2}^{\infty} \frac{ds}{s^2} K(s)R(s),$$

where

$$R(s) = \frac{\sigma(e^+e^- \rightarrow hadrons)}{e^+e^- \rightarrow \mu^+\mu^-},$$

with measured cross-sections $\sigma(e^+e^- \rightarrow hadrons)$ used as an input. Due to a $1/s^2$ factor the major part of integral comes from the low energies, where the $e^+e^- \rightarrow \pi^+\pi^-$ mode dominates $R(s)$. It turns out that $\sigma(e^+e^- \rightarrow \pi^+\pi^-)$ attributes to about 73% of $a_\mu^{had;LO}$.

^ae-mail: I.B.Logashenko@inp.nsk.su

The anomalous magnetic moment of muon was recently measured at BNL with 0.54 ppm precision [2]. This measurement generated high interest in a high precision measurement of $R(s)$, and, in particular, of $\sigma(e^+e^- \rightarrow \pi^+\pi^-)$. The most precise measurements with direct energy scan were done in the previous generation of experiments in Novosibirsk at the VEPP-2M collider with the CMD-2 and SND detectors. The high precision measurements of this mode were recently performed at KLOE and BaBar experiments using initial-state radiation (ISR) technique. The systematic error of all these measurements varies from 0.5% to 1.3% in the $\rho(770)$ resonance energy range. There is good overall agreement between different measurements, but there are local disagreements. The good reviews of the existing data are provided in the most recent calculations of the hadronic contribution to a_μ [4, 5]. Even at this percent level of accuracy, the systematic error of $\sigma(e^+e^- \rightarrow \pi^+\pi^-)$ gives the largest contribution of 0.27 ppm to the overall uncertainty of 0.43 ppm of the Standard model evaluation of a_μ .

The BNL measurement of a_μ is $2.2 \div 2.5$ ppm, or $3.3 \div 3.6$ standard deviations above the Standard Model expectation. This hint of the physics beyond SM was a strong motivation for a new experiment, now under construction at FNAL, which will measure a_μ with an accuracy of 0.15 ppm, about factor 4 improvement.

The CMD-3 goal is to measure the $e^+e^- \rightarrow \pi^+\pi^-$ cross section with a systematic uncertainty of 0.35% at $\sqrt{s} < 1$ GeV and moderately larger uncertainty at higher energies, which is about a factor of 2 improvement comparing with the previous measurement at CMD-2.

2 VEPP-2000 and CMD-3

The electron-positron collider VEPP-2000 [6, 7] was commissioned at Budker Institute of Nuclear Physics (Novosibirsk, Russia) in 2010. The machine covers the energy range from $\sqrt{s} = 0.32$ GeV to $\sqrt{s} = 2.0$ GeV. In order to reach the design luminosity in the single-bunch mode of $10^{32} \text{ cm}^{-2}\text{s}^{-1}$ at 2 GeV, the novel round beam technique is used.

Two detectors are installed in the two interaction regions of VEPP-2000 — CMD-3[8] and SND[9]. CMD-3 (Cryogenic Magnetic Detector) is a general purpose detector (Fig. 1). The tracks of charged particles are detected by the cylindrical drift chamber with hexagonal cells. The fiducial volume for charged tracks is precisely determined by the Z-chamber, a MWPC with dual anode and cathode readout. The barrel electromagnetic calorimeter, placed outside of the superconducting solenoid ($0.13X_0$, 13 kGs), consists of two systems: the Liquid Xenon calorimeter ($5.4X_0$), surrounded by the CsI crystal calorimeter ($8.1X_0$). The LXe calorimeter has 7 layers and utilizes dual readout: the anode signals are used for a measurement of the total energy deposition, while signals from the cathode strips provide information about a shower profile and are used for measurement of the coordinates of photons with high precision (about 1-2 mm). The endcap BGO crystal calorimeter ($13.4X_0$) operates in the main magnetic field. The time-of-flight system, designed to identify slow moving particles, is placed between the two layers of barrel calorimeter. The detector is surrounded by the muon range system.

The data taking has started at the end of 2010 and three independent data taking runs were performed so far. The whole available energy range was covered and about 60 pb^{-1} of integrated luminosity were collected by CMD-3. The physics program of experiments at VEPP-2000 includes a high precision measurement of cross sections of various modes of $e^+e^- \rightarrow \text{hadrons}$, studies of known and searches for new vector mesons, measurement of $n\bar{n}$ and $p\bar{p}$ production cross sections near threshold and searches for exotic hadrons

Two first data taking runs, 2011 and 2012, were focused on the energy range above the $\varphi(1020)$ meson, $\sqrt{s} > 1$ GeV. In 2013 the energy range below the $\varphi(1020)$ meson was scanned. Between 2012 and 2013 seasons there was an important upgrade of VEPP-2000 — the installation of the energy monitoring system[3], which continuously measures beam energy concurrently with data taking using back-scattered Compton photons. The results discussed here are based on the 2013 energy scan. The data were taken in 66 energy points at energies $0.32 < \sqrt{s} < 0.984$ GeV with an integrated luminosity of about 18 pb^{-1} , 8.3 pb^{-1} of which were taken at or near $\omega(782)$. The collected

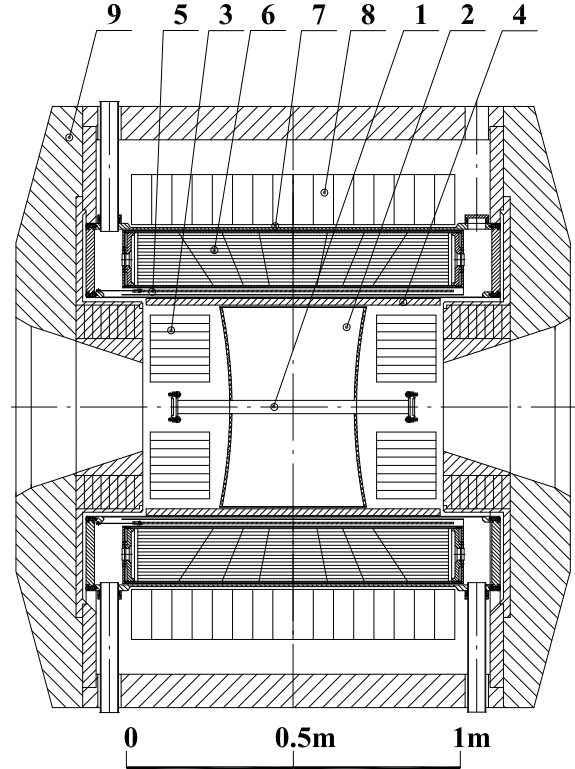


Figure 1. CMD-3 detector: 1 – beam pipe, 2 – drift chamber, 3 – BGO calorimeter, 4 – Z-chamber, 5 – superconducting solenoid, 6 – LXe calorimeter, 7 – TOF system, 8 – CsI calorimeter, 9 – yoke. Muon range system, not shown, is placed outside the yoke.

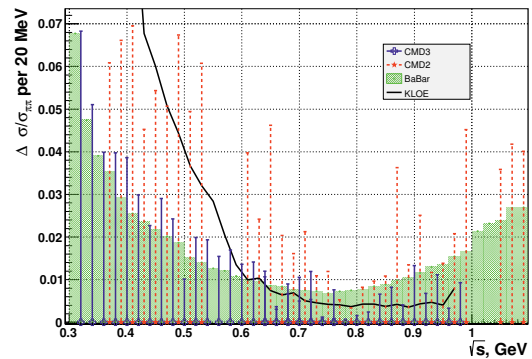


Figure 2. Expected relative statistical accuracy of $\sigma(e^+e^- \rightarrow \pi^+\pi^-)$ measured using CMD-3 2013 data in comparison with previous measurements

statistics are a few times that at CMD-2 and at the level of statistics collected at BaBar and KLOE (Fig. 2).

3 Data analysis

From $2 \cdot 10^9$ triggers about $1.8 \cdot 10^7$ were selected as *collinear* events with a signature of two back-to-back particles with opposite charges. The selection criteria include cuts on the average momentum p_{avr} of two particles, difference between two momenta Δp , acollinearity angles $\Delta\varphi$

and $\Delta\Theta$. The fiducial volume is determined by the cut on the average polar angle Θ of two particles:

$$1.1 \leq \frac{\Theta_1 + (\pi - \Theta_2)}{2} \leq (\pi - 1.1).$$

The selected sample consists of $e^+e^- \rightarrow e^+e^-, \mu^+\mu^-, \pi^+\pi^-$ pairs with small background ($\sim 1\%$) from cosmic events which pass near interaction point and are misidentified as collinear events. The number of background events is determined by the analysis of the spatial distribution of the vertex, which is close to uniform for cosmic events and peaked at the interaction point for beam-originated events.

The separation of different final states is based on binned likelihood minimization. Two independent approaches are used:

- the fit of two-dimensional momentum distribution

$$-\ln L = - \sum_{bins} n_i \ln \left[\sum_{X=ee,\mu\mu,\pi\pi,bg} N_X f_X(p^+, p^-) \right] + \sum_X N_X$$

where p^+ and p^- are the total momentum of a particle with positive and negative charge, respectively;

- the fit of two-dimensional energy deposition distribution

$$-\ln L = - \sum_{bins} n_i \ln \left[\sum_{X=ee,\mu\mu,\pi\pi,bg} N_X f_X(E^+, E^-) \right] + \sum_X N_X$$

where E^+ and E^- are the energy deposition in the barrel calorimeter of a particle with positive and negative charge, respectively.

Examples of the two-dimensional distributions used for separation of the final states are shown in Fig. 3. Several different methods are used to obtain p.d.f.s $f(E^+, E^-)$ and $f(p^+, p^-)$.

1. Background p.d.f.s $f_{bg}(E^+, E^-)$ and $f_{bg}(p^+, p^-)$ are obtained from the data using a sample of the cosmic muons which pass close enough to the beam axis, but outside the beam-crossing region. These events provide good representation of the background events in the collinears sample.
2. Momentum p.d.f.s $f_X(p^+, p^-)$ for electron-positron, muon and pion pairs are obtained from the Monte-Carlo. An ideal set of 2D distributions is generated with the MC code MCGPJ [10], which takes into account initial and final state radiation. The same selection cuts as for collinear events are applied. Then the ideal distributions are convoluted with the detector response functions, which take into account different tracker performance for electrons and MIPs. Some parameters of the detector response functions remain free during likelihood minimization.
3. Energy deposition p.d.f.s for electrons (positrons) $f_{ee}(E^+, E^-)$ are obtained from the data. The same sample of collinear events is used. A particle with high energy deposition is used to tag electron

(positron) on one side, which allows one to study the energy deposition of the opposite particle. The analytical model for $f_{ee}(E^+, E^-)$ has some parameters, which remain free during minimization.

4. Energy deposition p.d.f.s for muons $f_{\mu\mu}(E^+, E^-)$ are obtained from the Monte Carlo. A large sample of $e^+e^- \rightarrow \mu^+\mu^-$ events, 200000 per energy point, is generated with MCGPJ, selection cuts for collinear events are applied and the muons energy deposition is tabulated. Then the tabulated p.d.f.s are convoluted with calorimeter response, which allows to take into account difference between simulation and the data. The parameters of the response function remain free during minimization.
5. A very generic analytical model for energy deposition p.d.f.s of pions $f_{\pi\pi}(E^+, E^-)$ is used, which contains a contribution from minimum ionizing pions and pions, which have nuclear interactions in the detector. The model is validated with $\sim 10^6$ tagged pions, selected from $\omega \rightarrow 3\pi$ and $\varphi(1020) \rightarrow 3\pi$ decays, which cover practically all momentum and angle phase space important for this measurement.

The examples of the fits are demonstrated in Fig. 4 and Fig. 5.

The pion formfactor is calculated as:

$$|F_\pi|^2 = \frac{N_{\pi\pi}}{N_{ee}} \times \frac{\sigma_{ee} \cdot (1 + \delta_{ee}) \cdot \epsilon_{ee}}{\sigma_{\pi\pi} \cdot (1 + \delta_{\pi\pi}) \cdot \epsilon_{\pi\pi}} - \Delta_{3\pi},$$

where the ratio $N_{\pi\pi}/N_{ee}$ is obtained from the likelihood minimization, σ_X are the corresponding Born cross-sections, δ_X are the radiative corrections, ϵ_X are the detection efficiencies which include reconstruction and trigger efficiencies, Δ_D and Δ_N are the corrections for the pion losses caused by decays in flight and nuclear interactions respectively, and $\Delta_{3\pi}$ is the correction for misidentification of $\omega \rightarrow \pi^+\pi^-\pi^0$ events as $e^+e^- \rightarrow \pi^+\pi^-$. The cross section $\sigma(e^+e^- \rightarrow \pi^+\pi^-)$ is related to the pion formfactor as

$$\sigma(e^+e^- \rightarrow \pi^+\pi^-) = \frac{\pi\alpha^2}{3s} \beta_\pi^3 |F_\pi(s)|^2.$$

The ratio of the numbers of $\mu^+\mu^-$ and e^+e^- pairs, or the measured $e^+e^- \rightarrow \mu^+\mu^-$ cross-section, provides strong overall systematic test, as this ratio is well known from QED.

Radiative corrections were calculated using the MCGPJ generator [10] by the Monte Carlo integration of the differential cross sections imposing all selection criteria. The radiative corrections for the process $e^+e^- \rightarrow \pi^+\pi^-$ include the effects of both initial (ISR) and final state radiation (FSR) and do not include the vacuum polarization terms (both leptonic and hadronic) since the latter are considered to be an intrinsic part of the hadronic cross section. In contrast, the radiative corrections for $e^+e^- \rightarrow e^+e^-$ and $e^+e^- \rightarrow \mu^+\mu^-$ modes include all these contributions. However, when one measures the cross-section as a part of $R(s)$, the radiation of the final pions is no longer a radiative correction — $\pi^+\pi^-\gamma$ with a photon radiated by one

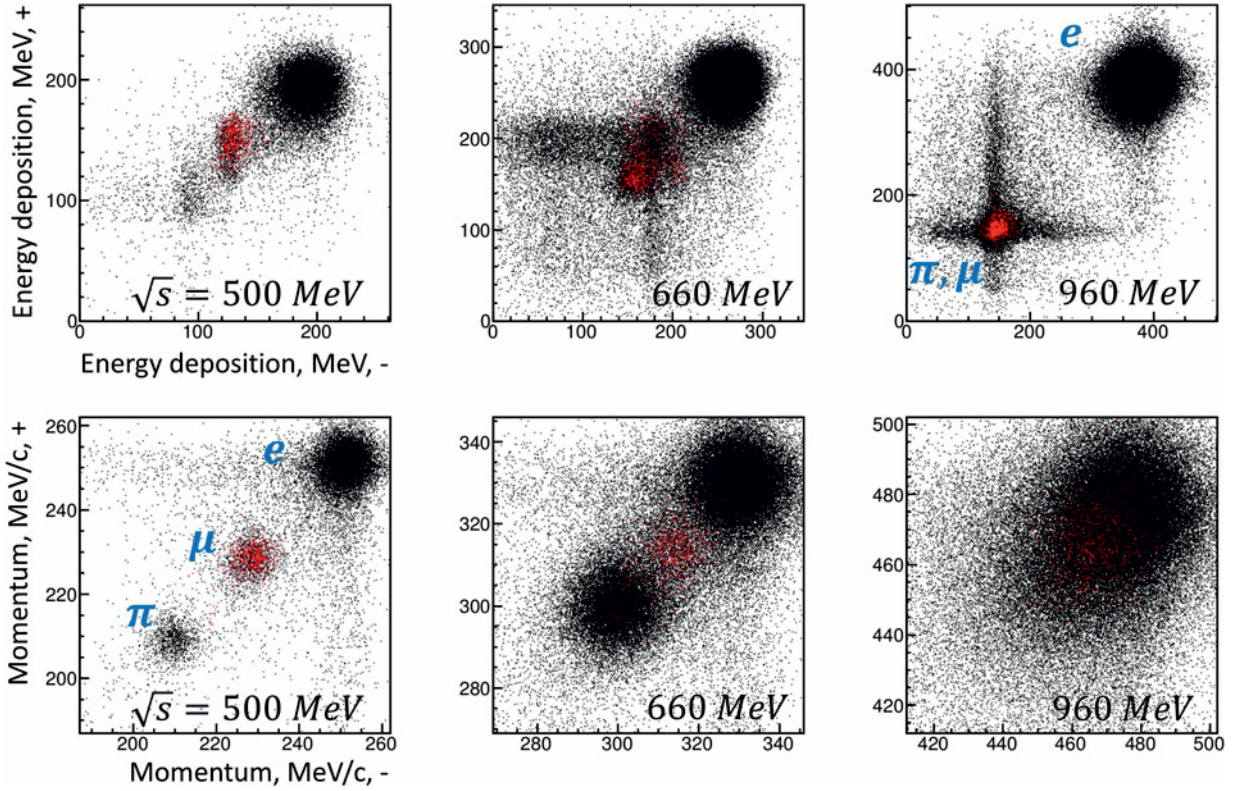


Figure 3. Examples of two-dimensional momentum and energy deposition distributions for energy points $\sqrt{s} = 500, 660, 960$ MeV. Black dots are data, red dots are simulation of $e^+e^- \rightarrow \mu^+\mu^-$. The energy distributions E^+ vs E^- are at the top, the momentum distributions p^+ vs p^- are at the bottom.

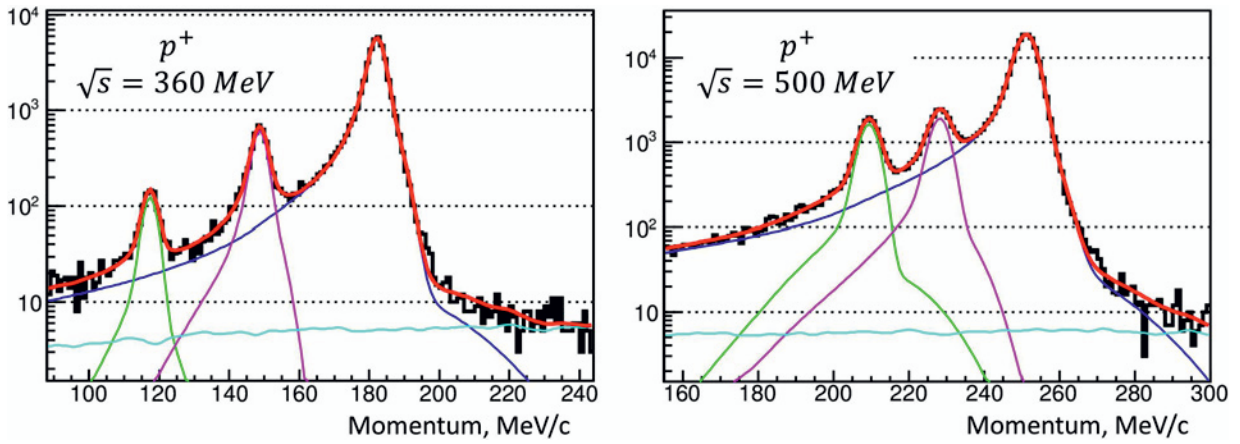


Figure 4. Example of the fit of the two-dimensional momentum distributions for energy points $\sqrt{s} = 360$ and 500 MeV. Black histogram is the data, red line is the fit. Contributions of e^+e^- (right peak), $\pi^+\pi^-$ (left peak), $\mu^+\mu^-$ (middle peak) final states and of the cosmic background (uniform-like) are also shown. Two dimensional distributions are used in fit. Here a one-dimensional p^+ projection of these distributions is shown for demonstration purpose.

of the final pions should be considered as one of the possible hadronic final states contributing to the total cross section. Moreover, the cross section, used in the $R(s)$ definition is the bare cross section, which does not include vacuum polarization. Therefore, when $R(s)$ is calculated, the following bare cross section $\sigma_{\pi\pi(\gamma)}^0$ should be used:

$$\sigma_{\pi\pi(\gamma)}^0 = \frac{\pi\alpha^2}{3s} \beta_\pi^3 |F_\pi(s)|^2 \cdot |1 - \Pi(s)|^2 \cdot \left(1 + \frac{\alpha}{\pi} \Lambda(s)\right),$$

where the $|1 - \Pi(s)|^2$ term excludes the effect of leptonic and hadronic vacuum polarization, and the $\Lambda(s)$ term is the FSR contribution in the approximation of the point-like pions.

The described approach to data analysis is similar to the one used in the previous CMD-2 measurement at VEPP-2M. Several detector advantages should allow to reach the higher precision at CMD-3: better resolution of

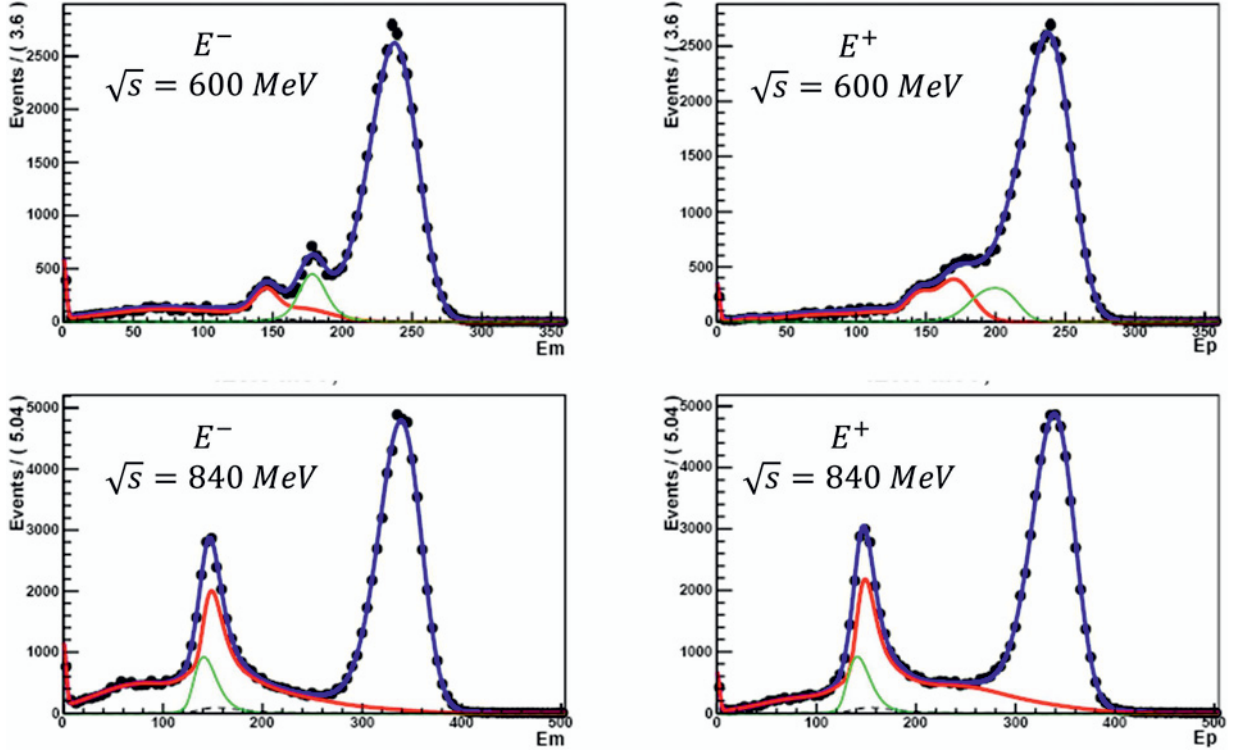


Figure 5. Example of the fit of the two-dimensional distributions of energy depositions for energy points $\sqrt{s} = 600$ and 840 MeV. Black points are the data, blue line is the fit. Contributions of $\pi^+\pi^-$ (red line), $\mu^+\mu^-$ (green line) final states and of the cosmic background (dashed line) are shown as well. Two dimensional distributions are used in fit. Here a one-dimensional projections of these distributions (E^- at the left and E^+ at the right) are shown for demonstration purpose.

the drift chamber and the barrel calorimeter, higher magnetic field, measurement of the shower profile with layered barrel calorimeter, etc. The main expected sources of the systematic errors are the following.

1. Event separation, 0.2%. Two independent ways of event separation provide important cross-check of systematic errors.
2. Detection efficiencies, 0.2%. Both the trigger, based on the tracker data, and the reconstruction software are highly efficient for collinear events ($\varepsilon > 99\%$). There is an independent trigger mode, which uses calorimeter data, which allows to monitor the trigger efficiencies. The reconstruction efficiency is monitored with specially selected sample of events. There are other contributions to detection efficiency, which are final state specific: bremsstrahlung of final electrons (positrons) on the beam pipe material, pion decays in flight, hadronic interactions on pions with the beam pipe material. All these corrections are of the order of 1%, are calculated via Monte-Carlo and partially confirmed with the data.
3. Fiducial volume, 0.1%. The detector construction allows for two independent ways for precise determination of the fiducial volume, using data from Z-chamber or LXe calorimeter. Mapping of detector elements using γ conversion and analysis of the an-

gular distribution of e^+e^- pairs provide additional systematic checks of acceptance.

4. Beam energy, 0.1%. For direct scan measurement, performed at CMD-3, it is important to know an average beam energy. A dedicated system, installed at VEPP-2000 at 2012, monitors beam energy in real time with 50 keV, well within requirements for cross-section measurement.
5. Radiative corrections, 0.1%. The corrections are calculated with the MCGPJ code, mentioned above. In order to reach the required precision, it will be important to compare it to other existing approaches and software packages [11] and to perform a detailed comparison of the radiative tails to the data.

The high statistics collected at CMD-3, a few times the CMD-2 data, allows one to perform more detailed systematic studies and to reach smaller systematic error.

4 Results and discussion

The preliminary results of the pion formfactor measurement are shown in Fig. 6. Efficiency corrections, expected at percent level, are not applied. At energies $\sqrt{s} < 0.6$ GeV the separation of the final states by momentum is the preferable approach, which provides stable results and allows to reach the best statistical error. The reasons are

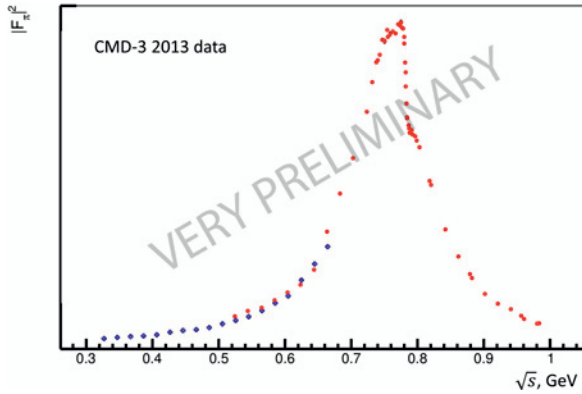


Figure 6. Preliminary results of the pion formfactor measurement using CMD-3 2013 data. Statistical errors are shown. Blue points — separation of the final states by momentum, red point — by energy deposition.

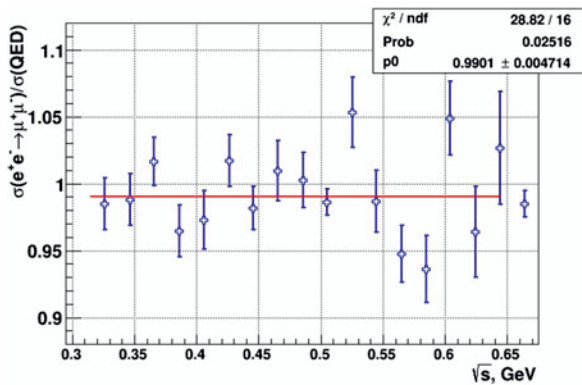


Figure 7. Ratio of the measured cross-section $e^+e^- \rightarrow \mu^+\mu^-$ to the QED expectation.

the corresponding p.d.f.s are well separated and have relatively simple structure, nicely reproduced with Monte-Carlo simulation. At energies $\sqrt{s} \gtrsim 0.7$ GeV the momentum resolution is not sufficient to clearly distinguish between e , μ and π , thus the separation of the final states by energy deposition is the preferable approach. This approach is applicable at lower energies as well, but its implementation becomes more complicated and fit becomes less stable because of the more complicated structure of the energy deposition of muons and pions. A possibility of incorporation of more variables in the likelihood fit, e.g. the shower profile or the scattering angle, is being investigated. That should help to increase the separation power and to extend applicability of particle separation by the

energy deposition to lower energies. In the intermediate region $0.6 \leq \sqrt{s} \leq 0.7$ GeV both approaches are used simultaneously and neither has clear advantage.

The ratio of $N_{\mu\mu}$ to N_{ee} for the analysis with momentum used for separation of the final states is shown in Fig. 7. This ratio is a powerful test of the overall procedure. Good agreement with the QED expectation is observed.

There are about 35 pb^{-1} collected at energies above $\sqrt{s} > 1$ GeV in 2011 and 2012. But these data were collected without beam energy monitoring system, and the trigger configuration, non-optimal for this kind of measurement, was used. We expect to collect an order of magnitude more data at these energies after VEPP-2000 upgrade, now underway, will be finished.

Acknowledgments

This work is supported in part by the RFBR grants 11-02-00112-a, 11-02-00328-a, 12-02-00065-a, 12-02-01032-a, 12-02-01250-a, 12-02-31498-mol-a, 12-02-31499-mol-a, 12-02-31501-mol-a, 13-02-00215-a, 14-02-00580-a and the DFG grant GZ: HA 1457/9-1.

References

- [1] T. Blum, A. Denig, I. Logashenko, E. de Rafael, B. Lee Roberts, T. Teubner and G. Venanzoni, arXiv:1311.2198 [hep-ph].
- [2] G. W. Bennett *et al.*, *Phys. Rev.* **D73** (2006) 072003.
- [3] E. V. Abakumova *et al.*, *Phys. Rev. Lett.* **110** (2013) 140402.
- [4] K. Hagiwara, R. Liao, A. D. Martin, D. Nomura, T. Teubner, *J. Phys. G* **38** (2011) 085003.
- [5] M. Davier, A. Hoecker, B. Malaescu, Z. Zhang, *Eur. Phys. J. C* **71** (2011) 1515, erratum *Eur. Phys. J. C* **72** (2012) 1874.
- [6] Yu. M. Shatunov *et al.*, *Conf. Proc. C* **0006262** (2000) 439.
- [7] D. Berkaev *et al.*, *Nucl. Phys. Proc. Suppl.* **225-227** (2012) 303.
- [8] B. I. Khazin *et al.*, *Nucl. Phys. Proc. Suppl.* **181-182** (2008) 376.
- [9] M. N. Achasov *et al.*, *Nucl. Instrum. Meth. A* **598** (2009) 31.
- [10] A. B. Arbuzov, G. V. Fedotov, F. V. Ignatov, E. A. Kuraev and A. L. Sibidanov, *Eur. Phys. J. C* **46**, 689 (2006) [hep-ph/0504233].
- [11] S. Actis *et al.*, *Eur. Phys. J. C* **66** (2010) 585.